Chem Soc Rev

Recent Advances in Controlled Synthesis of Two-Dimensional Transition Metal Dichacogenides via Vapour Deposition Techniques

Journal:	*Chemical Society Reviews*
Manuscript ID:	CS-TRV-07-2014-000256.R1
Article Type:	Review Article
Date Submitted by the Author:	28-Jul-2014

Complete List of Authors:	Shi, Yumeng; King Abdullah University of Science and Technology, Physical Science and Engineering LI, HENAN; Nanyang Technological University, School of Materials Science and Engineering Li, Lain-Jong; King Abdullah University of Science and Technology, Physical Science and Engineering

Chem Soc Rev

RSCPublishing

TUTORIAL REVIEW

Recent Advances in Controlled Synthesis of Two-Dimensional Transition Metal Dichacogenides *via* Vapour Deposition Techniques

Cite this: DOI: 10.1039/xoxxoooooox

Received 31th July 2014,
Accepted ooth January 2014

DOI: 10.1039/xoxxoooooox

www.rsc.org/

Yumeng Shi, [a] Henan Li, [b] and Lain-Jong Li, [a]*

Recent years there have been many breakthroughs in two-dimensional (2D) nanomaterials, among which the transition metal dichalcogenides (TMDs) attract significant attention owing to their unusual properties associated with their strictly defined dimensionalities. TMD materials with a generalized formula of MX_2, where M is a transition metal and X is a chalcogen, represent a diverse and largely untapped source of 2D systems. Semiconducting TMD monolayers such as MoS_2, $MoSe_2$, WSe_2 and WS_2 have been demonstrated to be feasible for future electronics and optoelectronics. The exotic electronic properties and high specific surface areas of 2D TMDs offer unlimited potential in various fields including sensing, catalysis, and energy storage applications. Very recently, the chemical vapour deposition technique (CVD) has shown great promise to generate high-quality TMD layers with scalable size, controllable thickness and excellent electronic properties. Wafer-scale deposition of mono to few layer TMD films have been obtained. Despite the initial success in the CVD synthesis of TMDs, substantial research works on extending the methodology open up a new way for substitution doping, formation of monolayer alloys and producing TMD stacking structures or superlattices. In this tutorial review, we will introduce the latest development of monolayer TMDs synthesis by CVD approaches.

1. Introduction

Two-dimensional (2D) transition metal dichalcogenides (TMDs)[1] have received much attention recently since they exhibit a wide range of unique electrical,[1, 2] optical,[3-5] thermal [6] and mechanical properties[7] that do not exist in their bulk counter parts. Monolayer molybdenum disulfide (MoS_2), one of the most frequently studied member of TMDs, exhibits not only good chemical stability and mechanical flexibility but also excellent optical and electrical properties.[8, 9] The semiconducting nature of MoS_2 ensures its high on/off current ratio and the presence of band gap emissions, while still sharing many of graphene's advantages for electronic and optoelectronic application.[10] The essential findings for these 2D materials enlighten researchers with innovations to develop future nanoelectronic devices that better serve the urging needs in compact, light-weight and high-performance integrated electronic systems.[8] The promising performance of the electronic and optoelectronic components made from TMD layers, such as field-effect transistors,[1, 10, 11] sensors[12, 13] and photodetectors,[2, 14, 15] proves them to be potential substitutes of Si in conventional electronics and of organic semiconductors in wearable and flexible systems. [16-19]

One major and very important research field of TMDs is the reliable production of atomically thin 2D layers and the manipulation of the electronic properties via scalable approaches. To date, two major strategies have been employed to obtain monolayer TMDs: one is the chemical[20-22] or mechanical exfoliation[23] from bulk crystals; the other is the bottom-up growth method. The top-down approaches allow to produce high-quality and micrometre-sized monolayers. It is generally believed, the mechanical exfoliated TMD monolayers possess higher quality and are clean on surfaces, suitable for fundamental research and proof-of-concept device fabrication. However, mechanical cleavage is not suitable for large scale production due to the absence of layer number control ability. On the other hand, chemical exfoliation of monolayer TMDs relies on the liquid-phase preparation method, which materials are promising for solution-based or printable electronics. Yet, the wet chemical method may unavoidably alter the lattice structure of thin TMD

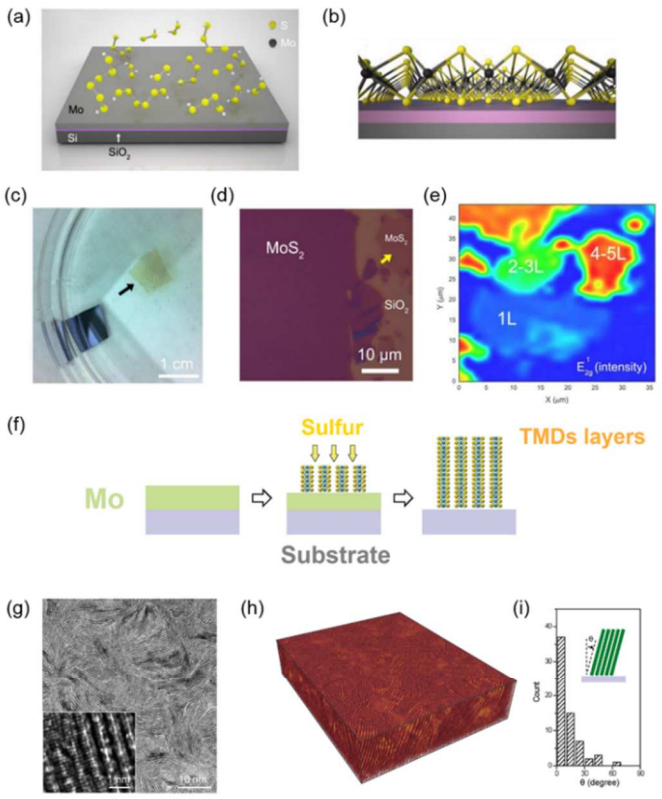

Fig. 1 (a) Illustrations of introducing sulfur to the Mo thin film which was pre-deposited on the SiO_2/Si substrate. [24] (b) The structure of MoS_2 on the substrates, where black and yellow atoms represent Mo and S, respectively. [24] (c) Peeled-off few-layer MoS_2 floating on the surface of water. [24] (d) Optical image of the edge of MoS_2 grown on the substrate. Area in dark purple colour are few-layer MoS_2. [24] (e) Typical landscape of MoS_2 atomic layers on SiO_2 substrates. The intensity of Raman E^1_{2g} mode is correlated to the number of layers. [24] Reproduced with permission from ref. 24. Copyright 2012, WILEY-VCH Verlag GmbH & Co. KGaA, Weinheim. (f) Schematically illustration of vertically grown TMDs. When the growth is limited by the diffusion of sulfur (selenium) gas, the TMD layers tend to be perpendicular to the substrate, with exposed van der Waals gap for fast reaction. [25] (g) TEM image of a MoS_2 film produced by rapid sulfurization, clearly showing exposed edges. High-resolution TEM image (inset) reveals individual layers consisting of three atomic planes in the sequence of S−Mo−S. [25] (h) Volume-rendered reconstructed TEM tomogram of a MoS_2 film grown by rapid sulfurization. [25] (i) Statistical distribution of tilt angles (θ) of layers in individual grains in edge-terminated MoS_2 film, where the tilt angle is defined in the inset. [25] Reproduced with permission from ref. 25. Copyright 2013, American Chemical Society.

layers or introduce extrinsic defects during the exfoliation process and thus require a post treatment to reconstruct the structure of monolayer TMDs. [20]

In this tutorial review, a comprehensive review for the synthetic routes and structural characteristics of monolayer TMD nanosheets and few layered nanoflakes, will be presented. The bottom-up synthetic routes including chemical vapour deposition (CVD), thermolysis, physical vapour transport and layer-by-layer conversion shall be discussed. The CVD approaches to synthesize TMD monolayer alloys and heterostructures are also introduced.

2. Bottom-up approaches towards controlled synthesis of TMDs

The synthesis of atomically thin TMDs with layer controllability and large-area uniformity is an essential requirement for practical application in electronic and optical devices. Huge efforts have been devoted to the controlled synthesis of 2D TMDs. The large-area and uniform synthesis of 2D TMDs in a controllable manner has remained as a challenge for a long time. Very recently, the CVD technique shows promise to generate high-quality TMD layers with scalable size, controllable thickness and excellent electronic properties. The obtained TMD monolayers or films can be used as the active components for nanoelectronics and as the building blocks for constructing layered heterostructures. For the time being, the CVD or similar method is likely the only available way for achieving wafer scale TMDs.

2.1 Synthesis of TMDs via Vapor Phase Deposition

(i) Sulfurization (or selenization) of metal (or metal oxide) thin film

There have been attempts to produce MoS_2 layers *via* simple sulfurization of Mo metal. In the report by Zhan *et al*,[24] Mo film was deposited on SiO_2/Si wafer and followed by thermal annealing in sulfur vapours to produce MoS_2 film (Fig. 1 a-e). The reaction mechanism for synthesizing MoS_2 could be simply understood as a direct chemical reaction. Therefore, the size and thickness of the pre-deposited Mo film determines the thickness and size of the obtained MoS_2 thin film. The direct sulfurization of Mo metal thin film provides a quick and easy way to access atomically thin MoS_2 layers on insolating substrates. However, due to the challenge of forming a uniform metal thin film, both single and few layer MoS_2 coexist on the substrates. The obtained MoS_2 layers show a metallic transport property with a low on/off current ratio, which could be due to the presence of unreacted metal impurities.

Similarly, Kong *et al.* reported that the vertically aligned MoS_2 and molybdenum diselenide ($MoSe_2$) layers can be produced by a rapid sulfurization/selenization process at 550 °C (Fig.1 f-i).[25] Smooth and uniform TMD edge-terminated films with densely packed, strip-like grains can be produced on various substrates including glassy carbon, quartz and oxidized silicon. It is suggested that the distinction between vertical and in-plane growth of TMDs could be due to different sulfurization/selenization conditions. The formation of the vertically aligned TMD layers is proposed to be driven by a kinetic process, where at a high temperature the transition metal thin film converts to sulfide/selenide much faster than the diffusion of sulfur/selenium. Thus the sulfur/selenium diffusion limits the growth process. On the other hand, the anisotropic structure of TMD layers, makes it much faster for sulfur/selenium diffusion along the van der Waals gaps. Therefore, the TMD layers naturally orient perpendicular to the film, exposing van der Waals gaps for fast reaction.[25] These TMD layers with predominately exposed edges exhibit high surface energy and are thought to be metastable which may serve for diverse catalytic reactions.

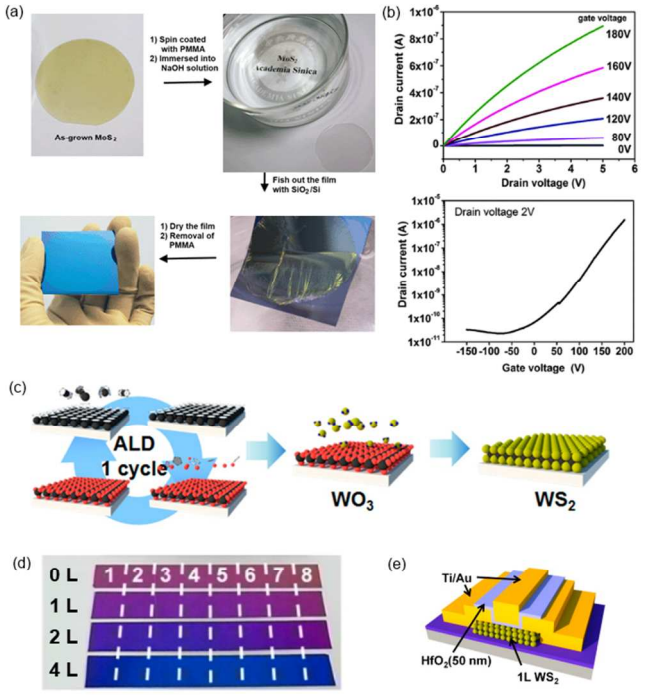

Fig. 2 (a) Pictures showing the procedure to transfer as-synthesized MoS_2 layer from a sapphire to a SiO_2/Si substrate. [26] (b) Output characteristics (drain current I_d *vs.* drain voltage V_d) and transfer curves (I_d *vs.* gate voltage V_g) for the bottom-gate transistor based on the MoS_2 layers. [26] Reproduced with permission from ref. 26. Copyright 2012, Royal Society of Chemistry. (c) Schematic illustration of the synthetic procedure for the ALD-based WS_2 nanosheets. [28] (d) Optical image of the transferred WS_2 on the SiO_2 substrate. The colour change from light purple to dark blue suggests the increased layer number of WS_2 as indicated in the figure. [28] (e) Typical FET device structure based on the WS_2 atomic layers. [28] Reproduced with permission from ref. 28. Copyright 2013, American Chemical Society.

An alternative effort has also been devoted to producing wafer-scale semiconducting MoS_2 thin layers,[26] where the direct sulfurization approach is adapted but replacing the Mo metal with MoO_3 thin layer (Fig. 2 a-b). The MoS_2 thin film derived from this method shows a high on/off current ratio rather than the resistor-like behaviour. To produce wafer-scale MoS_2 thin film, MoO_3 thin layer with a desired thickness was firstly prepared by thermal evaporation on sapphire substrates. During the growth, MoO_3-coated sapphire substrate was initially reduced to MoO_2 or other reduced Mo forms in a H_2/Ar environment at 500 °C. The sample was then annealed in a sulfur-rich environment at 1000 °C, which leads to the formation of wafer scale MoS_2 thin layer with semiconductor properties. The as-grown MoS_2 thin film can be transferred to arbitrary substrates for electronic device fabrication, thus the target substrate does not need to expose to high temperatures. Similar strategy has also been adoped for the synthesis of large-area WS_2 sheets with controllable thickness.[27]Although it is still at its infant stage, this approach paves a practical way to the synthesis of TMD films for large scale integrated electronics and optoelectronics.

The aforementioned TMDs synthesis method by direct sulfurization (or selenization) of transition metal (or metal oxide) thin film has several limitations, for example, it is hard to control the thickness of pre-deposited metal oxide or metal thin film, which limits the wafer-scale uniformity. To obtain a high-quality TMD with desired number of layers, the thickness of metal oxides need to be precisely controlled. Recent attempts have been made to improve the synthetic

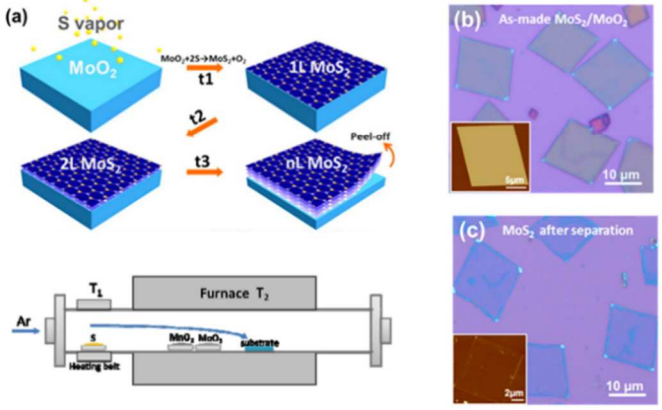

Fig. 3 (a) Schematics for the synthesis and cleavage of MoS_2. MoO_2 microplates were synthesized by the reduction of MoO_3 and then used as templates to grow MoS_2 *via* layer-by-layer surface sulfurization. [29] (b) and (c) Pictures showing the as-synthesized MoS_2/MoO_2 layers on SiO_2/Si wafer and the peeled off MoS_2 layers after removing MoO_2. Insets display the atomic force microscope (AFM) images of as-produced MoS_2/MoO_2 plates and the transferred MoS_2 flakes, respectively. [29] Reproduced with permission from ref. 29. Copyright 2013 American Chemical Society.

process by depositing metal oxides layer *via* atomic layer deposition (ALD).[28] By this method, atomically thin TMD nanosheets with systematic thickness controllability and wafer scale uniformity can be achieved (Fig. 2 c-e). Song *et al.* demonstrated that the number of tungsten disulfide (WS_2) layers can be controlled by tuning the number of cycles of ALD tungsten trioxide (WO_3).[28] Because ALD is used for the metal oxide deposition, the obtained TMDs retain the benefits of the ALD process including thickness controllability, reproducibility, wafer scale uniformity and high conformality. Yet the precursor $WH_2(iPrCp)_2$ used for the forming of metal oxides is not readily and widely available and the growth could also be limited to certain substrates, for example, the chemically inert and hydrophobic substrates may not be able to efficiently initiate the growth of WO_3 by ALD.

In the above mentioned TMD thin layers, formation of TMD thin films are realized by the sulfurization/selenization reaction or thermal decomposition of the pre-deposited precursors such as Mo, and MoO_3 on the growth substrates. Obviously, the growth of 2D TMD layers can be simplified as deposition of the precursors and large-area thin film can be produced subsequently. However the TMD layers are mostly polycrystalline with a small crystal grain size and uncontrollable layer number. To address this issue, Wang *et al.* reported a method capable of producing highly crystalline MoS_2 flakes with controlled number of layers by using MoO_2 microcrystals as templates (Fig. 3).[29] In this method, MoO_2 rhomboidal microplates were firstly synthesized by thermal evaporation of MoO_3 powder in sulfur environment at 650-850 °C. The surface of MoO_2 microplates was further sulfurized to MoS_2 at a higher temperature (850 – 950 °C) at a later stage. The resulting MoS_2 thin layers can be peeled off from MoO_2 microcrystals using polymethylmethacrylate (PMMA) mediated transfer printing method.[29] The surface sulfurization of crystalline MoO_2 microplates produces a top MoS_2 layer with a high crystallinity. The efficiency of sulfurization was limited by the diffusion rate of sulfur atoms through the existing MoS_2 outer layer. Thus the layer-by-layer sulfurization is possible by adjusting the sulfurization conditions. However, the MoS_2 growth is still determined by the crystal size of MoO_2 flakes, where the MoS_2 single crystal obtained are randomly distributed as isolated islands. Also, the peeling and transfer process

could generally lead to the damage of the MoS_2 surfaces and degradation of its electronic properties.

(ii) Thermal decomposition of thiosalts

In order to produce large-area, uniform and high-quality TMD sheets with good electrical performance, efforts have been devoted to the thermolysis of the precursor containing Mo and S atoms. In 2011, Li's group reported a two-step thermolysis process of ammonium thiomolybdate was able to produce highly crystalline and large-area MoS_2 thin sheets on a variety of insulating substrates (Fig. 4 a). [30] For the first time, the field-effect transistors (FETs) devices based on the CVD derived MoS_2 films exhibit high on/off current ratio and excellent carrier mobility values that are comparable with those obtained from the micromechanical exfoliated MoS_2 thin sheets.[1] The thermolysis of the single precursor ammonium thiomolybdate $(NH_4)_2MoS_4$ dissociated it to MoS_2, NH_3 and S vapors at above 800 °C. The transformation process of $(NH_4)_2MoS_4$ to MoS_2 involves many steps and the presence of oxygen may significantly affect the reaction. Nevertheless, ammonium thiomolybdate needs to be dissolved in polar organic solvents, the carbon contaminations from the residual solvent molecules could also cause the sulfur deficit in the final composition. Therefore, a two-step annealing process is developed to produce high-quality MoS_2 thin film. The $(NH_4)_2MoS_4$ thin film was firstly prepared by dip-coating method and carried in to a quartz tube chamber with the Ar/H_2 flow. Temperature was elevated to 500 °C to efficiently remove the residual solvents, NH_3 molecules and other by-products dissociated from the precursors. For the second step, temperature was raised to 1000 °C and the sulfur vapours were introduced. It was suggested that the conversion of $(NH_4)_2MoS_4$ to MoS_2 completed at ~425 °C. However, the addition of sulfur during the second annealing process removes the oxygen-containing defects and improves the crystallinity of MoS_2 thin film. The transistor devices fabricated with MoS_2 thin layers in a bottom gate geometry exhibit *n*-type behaviours with a significantly improved on/off current ratio which is $\sim 10^5$ and the field-effect electron mobility is up to 6 $cm^2/(V\ s)$.

Based on this film, MoS_2 electric double-layer transistors (EDLTs) formed with an ionic liquid were developed. (Fig. 4 b-g)[11, 31] These thin-film MoS_2 transistors exhibit remarkably high mechanical flexibility, where the electrical characteristics do not significantly change with bending. Most importantly, these MoS_2 based field effect transistors show excellent band transport with a low threshold voltage (<1 V) and high mobility (12.5 $cm^2/(V•s)$). Although the thermolysis of ammonium thiomolybdate produces high quality of MoS_2 thin film, synthesis of large area TMDs by this method is still challenging due to the technical limitation of uniform and ultra-thin ammonium thiomolybdate film preparation. Meanwhile, the as-synthesized films are polycrystalline.

(iii) Vapour phase reaction of transition metal oxides with chalcogen precursors

A very early strategy for growing large-area MoS_2 atomic layers reported by Li's group is based on the direct chemical vapour phase reaction of MoO_3 and S powders.[32, 33] During the MoS_2 growth, MoO_3 in vapour phase undergoes a two-step reaction, where MoO_{3-x} is likely formed during the reaction as an intermediate phase and these suboxide compounds diffuse to the substrate and further react with sulfur vapours to grow MoS_2 layers. This method allows the growth of single-crystalline MoS_2 flakes directly on arbitrary substrates depending on the control of nucleation density. Hence this

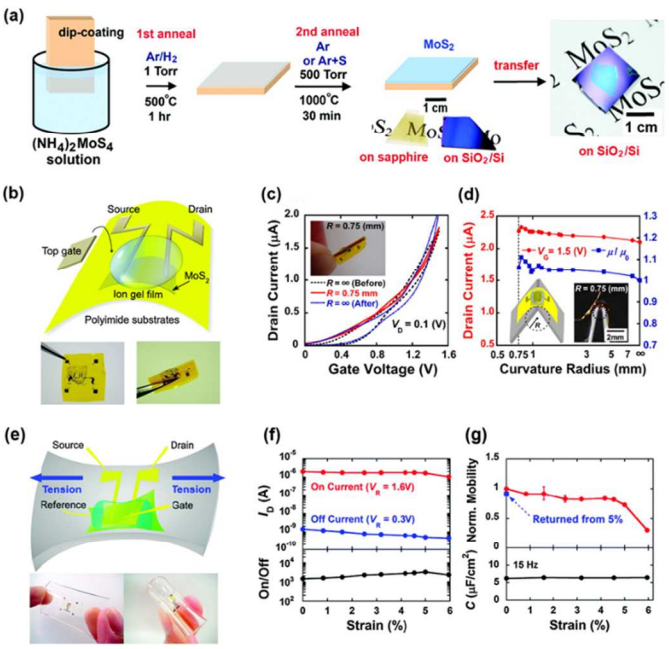

Fig. 4 (a) Schematic illustration of the two-step thermolysis synthesis of MoS_2 thin layers on insulating substrates. The precursor $(NH_4)_2MoS_4$ was dip-coated on SiO_2/Si or sapphire substrates followed by the two-step annealing process. The as-grown MoS_2 film can be transferred onto other arbitrary substrates. Pictures showing the procedure to transfer as-synthesized MoS_2 layer from a sapphire to a SiO_2/Si wafer. [30] Reproduced with permission from ref. 30. Copyright 2012 American Chemical Society. (b) Schematic depiction and optical images of the MoS_2 EDLT. [11] (c) Transfer characteristics of the MoS_2 EDLT. The red, black dotted and blue dotted lines correspond to the transfer curve for a curvature radius of 0.75 mm and the transfer curves before and after the bending experiments, respectively. The inset shows the optical image of the 0.75 mm curvature radius. [11] (d) The dependence of the drain current at a gate voltage of 1.5 V (red) and the carrier mobility on the curvature radius. The carrier mobility is normalized by the results without bending (blue). The inset schematically illustrates the bending measurement. [11] Reproduced with permission from ref. 11. Copyright 2012 American Chemical Society. (e) Schematic illustration and optical images of the MoS_2 transistor under stretching. [31] (f) Top and bottom respectively show the strain dependence of the drain current and on/off current ratio under different reference voltages. [31] (g) Top: electron mobility at various strains. Bottom: the specific capacitance of the ion-gel/MoS_2 interface at 15 Hz under various strains.[31] Reproduced with permission from ref. 31. Copyright 2013, AIP Publishing LLC.

method has been widely used for producing synthetic TMD monolayers.

The growth of MoS_2 is very sensitive to the substrate treatment prior to the growth.[32] The facilitated nucleation by seeding the substrate with graphene-like species has been explored (Fig. 5). [32-34] The substrate treatment using aromatic molecules, such as reduced graphene oxide (r-GO), perylene-3,4,9,10-tetracarboxylic acid tetrapotassium salt (PTAS) and perylene-3,4,9,10-tetracarboxylic dianhydride (PTCDA), promotes the lateral growth of MoS_2. These graphene-like molecules act as the seeds for growing MoS_2 thin layers. In their growth, the seed concentration is essential for the growth of large-area, continuous and high-quality MoS_2 monolayer. Very recently, the role of various seeding promoters in MoS_2 growth was further studied in details.[34] Aromatic molecules, such as copper(II) 1,2,3,4,8,9,10,11,15,16,17,18,22,23,24,25-hexadecafluoro-29H,31H-phthalocyanine ($F_{16}CuPc$), copper

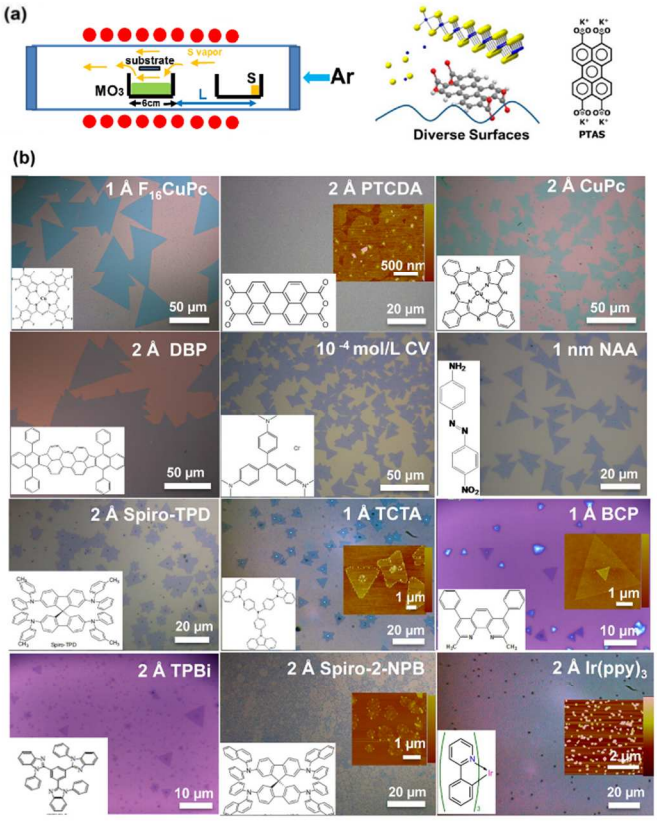

Fig. 5 (a) Schematics for the experimental setup and the growth process on diverse surfaces. The chemical structure of PTAS is shown on the right. [332] Reproduced with permission from ref. 33. Copyright 2013 American Chemical Society. (b) Pictures showing the quality of MoS_2 layers synthesized on SiO_2/Si substrates by using various small molecule promoters. The triangular shape of most crystallites reflects the 3-fold symmetry of MoS_2 suggesting they are single-crystalline. Insets display the corresponding growth promoters and some of the typical AFM images of as-made MoS_2 layers, respectively. [34] Reproduced with permission from ref. 34. Copyright 2014 American Chemical Society.

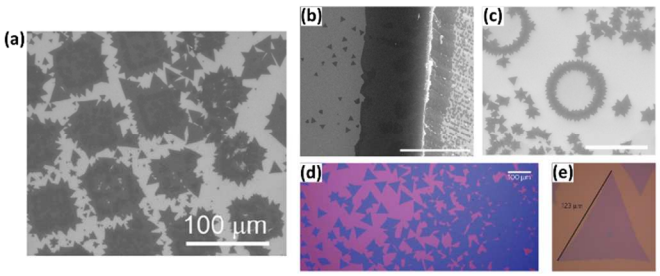

Fig. 6 (a) Scanning electron microscope (SEM) image demonstrating MoS_2 synthesis using rectangular patterns. [35] (b) SEM image shows the affinity of nucleation to the edges and rough surfaces. A higher density of nucleation is frequently observed on the cross-sectional surface and at substrate edges. [35] (c) Induced nucleation of MoS_2 domains near artificially-made circular edges on SiO_2. [35] Reproduced with permission from ref. 35. Copyright 2013 Macmillan Publishers Limited. (d) Optical image of large-grain MoS_2 grown by CVD method. [36] (e) A MoS_2 triangle measured up to ~120 µm from tip to tip. [36] Reproduced with permission from ref. 36. Copyright 2013 Macmillan Publishers Limited.

phthalocyanine (CuPc) and dibenzo{[f,f′]-4,4′,7,7′-tetraphenyl-diindeno [1,2,3-cd:1′,2′,3′-lm]perylene (DBP) can facilitate the growth of large-area, high-quality and continuous monolayer MoS_2. However, when inorganic seeding promoters including aluminum oxide (Al_2O_3), hafnium oxide (HfO_2) and SiO_2 are used, no monolayer MoS_2 can be found on the substrates after the growth.

It is anticipated that the presence of aromatic molecules provides a better wetting of the growth surface and lowers the free energy for the nucleation. Among the organic promoters, PTAS as a seeding promoter works exceedingly well for promoting MoS_2 growth on hydrophilic substrates, while $F_{16}CuPc$ is found to be a promising seeding promoter for the growth of MoS_2 uniformly on hydrophobic substrates, $F_{16}CuPc$ can significantly promote the heterogeneous nucleation process and allowing the fabrication of hybrid structures between MoS_2 monolayers, *h*-BN and graphene (graphite).

Najmaei *et al*. used MoO_3 nanoribbons and sulfur as the reactants for MoS_2 growth.[35] It is found that the MoS_2 triangular crystals are commonly nucleated and formed on the step edges (Fig. 6 a-c). By patterning the substrates using conventional lithography processes, the nucleation of MoS_2 layers can be controlled (Fig. 6 a). The edge-dominated catalytic process is due to a significant reduction in the nucleation energy barrier of MoS_2 at step edges as compared with the flat surface (Fig. 6 b).[35] Further experiments reveal that small triangular MoS_2 domains are preferentially nucleated at the step edges (Fig. 6 c) and then continue to grow and formed boundaries with other domains. The coalescence finally results in a continuous MoS_2 film (Fig. 6 d). [36] It is also found the coalescence of the grains could either leads to the chemically bounded grain boundaries or the grains are simply jointed together by growing on top of each other, without forming any chemical bonds.

Van der Zande *et al*. reported a refined route for ultra-large MoS_2 single crystal growth with solid MoO_3 and S precursors.[36] The highly crystalline islands of monolayer MoS_2 can be up to 120 µm in lateral size (Fig.6 e). Neither seeding molecules nor step-edge were used to promote the nucleation of MoS_2. Large MoS_2 crystalline islands with average size between 20 and 100 µm were obtained by using ultraclean substrates and fresh precursors. The yield can be significantly decreased if dirty substrates or old precursors are used according to the report.

The direct sulfurization/selenation of various metal oxides or metal chlorides[37] have been widely applied in many research groups to produce TMD layers such as MoS_2,[18, 37] WS_2,[27, 38, 39] $MoSe_2$[40, 41] and WSe_2.[42] Among the numerous reports on the synthesis of sulfides and selenides, one should notice that for selenides synthesis H_2 gas is commonly introduced as an additional reducing agent along with Se to further reduce the metal oxides and assist the selenization reaction.[39, 42] Furthermore, Zhang *et al*. revealed that minor H_2 carrier gas can also tailor the shape of monolayer WS_2 from jagged to straight edge triangles under low pressure chemical vapour deposition.[39]

(iv) Vapour phase transport and recrystallization from TMD powders

The chemical vapour phase reaction of metal oxides and sulfur/selenium yields monolayers of TMDs which are suitable for FETs fabrication. Yet both tilt and mirror twin boundaries are commonly found in the CVD TMD layers.[35, 36, 39] It has been proved intervalley scattering enhanced by defects and impurities can reduce or destroy the valley polarization.[3, 43, 44] Thus a method for producing high optical quality monolayer TMDs is required for investigating valley-related physics.

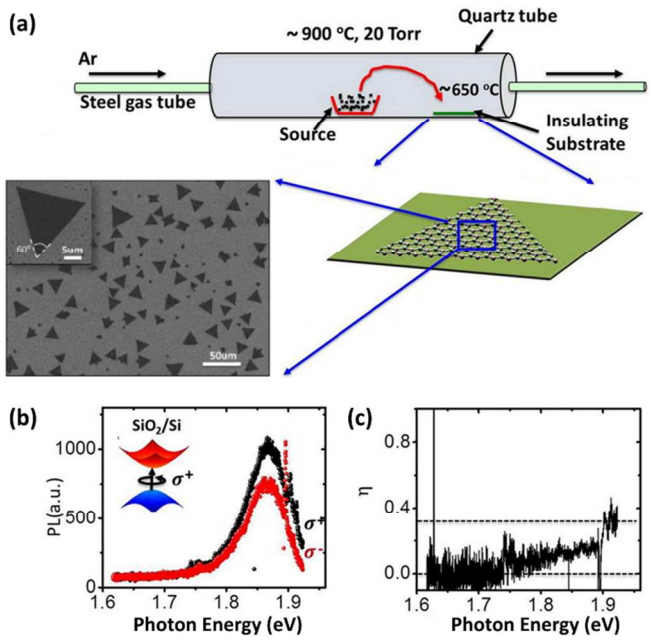

Fig. 7 (a) schematic illustration of experimental setup and SEM images of the as grown MoS_2 layers using vapour phase transport methods. [44] (b) σ^+ and σ^- components of the PL for monolayer VS synthesized MoS_2 on SiO_2/Si substrate, [44] (c) degree of PL circular polarization *vs.* photon energy (eV) at room temperature.[44] Reproduced with permission from ref. 44. Copyright 2013 American Chemical Society

Wu *et al*. have developed a vapour-solid (VS) growth method for synthesizing high optical quality MoS_2 monolayer.[44] MoS_2 monolayer flakes can be produced on insulating substrates (such as Si wafer and sapphire) by simple physical vapour transport of MoS_2 powder in an inert environment. MoS_2 power was evaporated at ~ 900 °C under a low pressure of 20 torr. The collecting substrates were put in a heating zone at 650 °C (Fig.7 a). It has been reported that the intervalley scattering increases with temperature due to the enhanced phonon populations, resulting in the decrease of valley polarization. The photoluminescence (PL) polarization obtained from the MoS_2 prepared by VS growth is substantial with a maximum of 35% at ~1.92 eV, even at room temperature. The result suggests the VS grown MoS_2 has a superb optical quality and high crystallinity (Fig. 7 b-c). However, for the VS growth the nucleation of MoS_2 crystals appears to be random and thicker layers of MoS_2 can also be frequently found, which is due to the limitation of VS growth technique.

2.2 Synthesis of band gap tuneable monolayer alloys

Bandgap engineering of 2D materials is critical to their applications in nanoelectronics and optoelectronics. Tuning band energies of TMDs can be achieved through strain engineering, the reported tunability of the band gap is within 100 meV per 1% strain. [45-47] However, the strain engineering remains difficult to be utilized for real electronic devices fabrication. Alternatively, the metallic or semiconducting properties of TMDs can be determined by the choice of transition metals and the substitution doping of chalcogenides also gives the freedom of tuning the electronic properties. [48] In other words, the intrinsic band gap of TMDs can be engineered by stoichiometry. Fortunately, the isomorphism of the transition metal dichalcogenide families (MX_2:M=Mo, W; X=S, Se, Te) also makes them promising candidates to form ternary van der Waals alloys without phase separation.[49-53]

In early studies, the TMD solid solutions both in the metal (e.g., $Mo_xW_{1-x}S_2$) and chalcogen (e.g., $MoS_{2(1-x)}$ Se_{2x}) sublattice forms have been realized by the direct vapour transport growth, where the stoichiometric amounts of desired powder elements were introduced into a quartz ampoule for crystal growth.[49-52] Very recently, the transition-metal dichalcogenide monolayer alloys ($Mo_{1-x}W_xS_2$) have been obtained by mechanical cleaving from their bulk crystals,[51] where a tuneable band gap emission ranging from 1.82 eV to 1.99 eV was obtained. The theoretical calculations show that the mono layers of ternary van der Waals alloys, such as $MoS_{2x}Se_{2(1-x)}$ are thermodynamically stable at room temperature.[48] Therefore, it is possible to directly produce single layer ternary TMD alloys *via* the

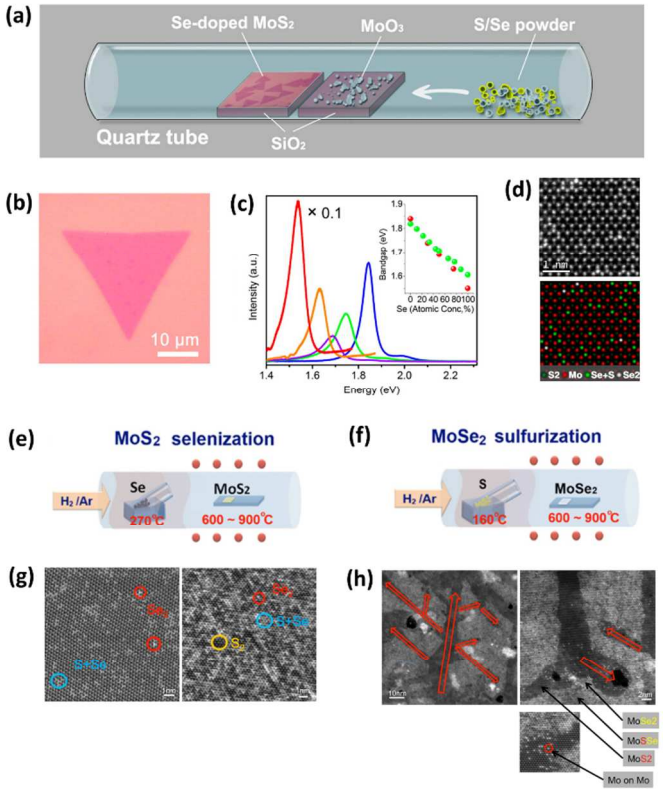

Fig. 8 (a) schematically illustration of the controlled synthesis of $MoS_{2(1-x)}Se_{2x}$ layers via chemical vapour deposition. [53] (b) Typical optical images of monolayer and single-crystal domains. [53] (c) PL spectra change showing the modification of the optical (excitonic) gap in MoS_2 as a function of Se doping. As the Se concentration increases, a noticeable red-shift in the peak position from 670 to 805 nm is observed, corresponding to an optical gap change from 1.85 to 1.54 eV. [53] (d) Structure model showing the distribution of single- and double-Se substituted S_2 sites. [53] Reproduced with permission from ref. 53.Copyright 2013 American Chemical Society (e) and (f) Schematic illustration of the experimental set-up for the selenization and sulfurization process, where the inlet gas carries the vaporized selenium (or sulphur) to the heated MoS_2 (or $MoSe_2$)flakes. [56] (g) TEM images of the selenized MoS_2 flakes. Large numbers of S_2, Se_2 and S-Se can be identified and the replacement is generally homogeneous in location. [56] (h) TEM image of $MoSe_2$ sulfurized at 700°C. The field is composed of two obvious MoS_2 and $MoSe_2$ domains, where MoSSe domains are also found in some area. The sulfurization preferentially proceeds through certain directions, which are related to the crystal orientation. [56] Reproduced with permission from ref. 56. Copyright 2014 Su, Hsu, Hsu, Chen, Chiu, Lin, Chang, Suenaga, He and Li.

bottom up technique. By adapting the VS growth approach, Feng *et al*. reported the growth of 2D $MoS_{2(1-x)}Se_{2x}$ ($0 \leqslant x \leqslant 0.40$) semiconductor alloys.[54] MoS_2 and $MoSe_2$ powders are used as the growth precursors and simultaneously evaporated to form the TMD alloys under a pressure of ~8 Pa.[54] By tuning the evaporation temperature of MoS_2 and $MoSe_2$, the composition of as-synthesized $MoS_{2(1-x)}Se_{2x}$ monolayers can be controlled. Furthermore, the bandgap photoluminescence is tunable from 1.86 eV (i.e., 665 nm, reached with x = 0) to 1.73 eV (i.e., 716 nm, reached with x = 0.40).[54]

Gong *et al*. utilized the same technique developed for MoS_2 and WS_2 synthesis to produce ternary van der Waals alloys where selenium and sulfur were mixed with a certain weight percentage to react with MoO_3 (Fig. 8 a-d).[53] It was found the doping of Se in MoS_2 layer is random and homogeneous at the nanoscale. PL measurement shows that the optical band gap of $MoS_{2(1-x)}Se_{2x}$ can be continuously tuned between 1.85 eV and 1.60 eV by changing the Se doping level. However, large variations in atomic composition from flakes to flakes are expected owing to the difficulty to precisely control the S and Se vapour diffusion in a small CVD furnace. A scalable method to synthesize monolayer TMD alloys is still urgently needed for practical applications.

Su *et al*. systematically compared the two approaches of forming $MoS_{2x}Se_{2(1-x)}$ monolayer alloys: selenization of CVD MoS_2 and sulfurization of CVD $MoSe_2$ (Fig. 8 e-h). [55, 56] The optical energy gap of as-grown MoS_2 can be continuously modulated from 1.86 eV to 1.57 eV depending on the reaction temperature. Spectroscopic and TEM evidences show that the Mo-S bonds can be replaced by the Mo-Se bonds in a random manner. In contrast, the replacement of Mo-Se by Mo-S preferentially occurs along certain directions depending on the crystalline orientation of $MoSe_2$ and thus the $MoSe_2/MoS_2$ biphases can be observed in the alloys, which makes the optical band gap of these alloys distinctly different. The study suggests that the reaction is kinetically controlled and the temperature is a straightforward control parameter for the composition of monolayer alloys.

2.3 Heterostructural stacking based on MoS_2 and other 2D monolayers

With various 2D building blocks in hand, it is possible to create novel atomically thin crystals *via* stacking various materials such as graphene, *h*-BN and TMDs with proper procedures. Combining the electronic properties of different 2D layered materials in hybrid heterostructures offers the possibility to create devices with new functionalities. Therefore, it is of huge interest in the construction of these hetero-layered materials, e.g. alternating individual layers of different 2D films (Graphene, boron nitride, Mica, MoS_2, WS_2, WSe_2 and $MoSe_2$) with particular stacking patterns. Depending on the interlayer coupling strength, the luminescence spectrum of TMDs can be tailored.[57] These TMD tandem structures provide unlimited opportunities to develop unique properties for both fundamental study as well as electronic and photovoltaic applications.

Many novel devices are based on heterostructures formed between MoS_2 and graphene. Electronic logic and memory devices have already been constructed from graphene–MoS_2 hybrids. [58, 59] The graphene/MoS_2 heterostructures have also been adopted to demonstrate an extremely high photo gain [4, 60] and the ultrasensitive detection of DNA hybridization. [61] Therefore, efforts have also been made in the growth of hybrid graphene/MoS_2 structures. Lin et al. reported the direct synthesis of TMDs on epitaxial graphene, these large-area van der Waals heterostructures show a significant improvement in photoresponse compared to the TMD layer along.[60] Shi *et al*. reported the self-assemble of MoS_2 flakes on the graphene surface via thermal decomposition of ammonium thiomolybdate (Fig. 9 a).[62] Notice that the lattice spacing for MoS_2 is 28% larger than that for graphene, it is likely that the crystal orientation can be incommensurate due to the large strains between layers. However,

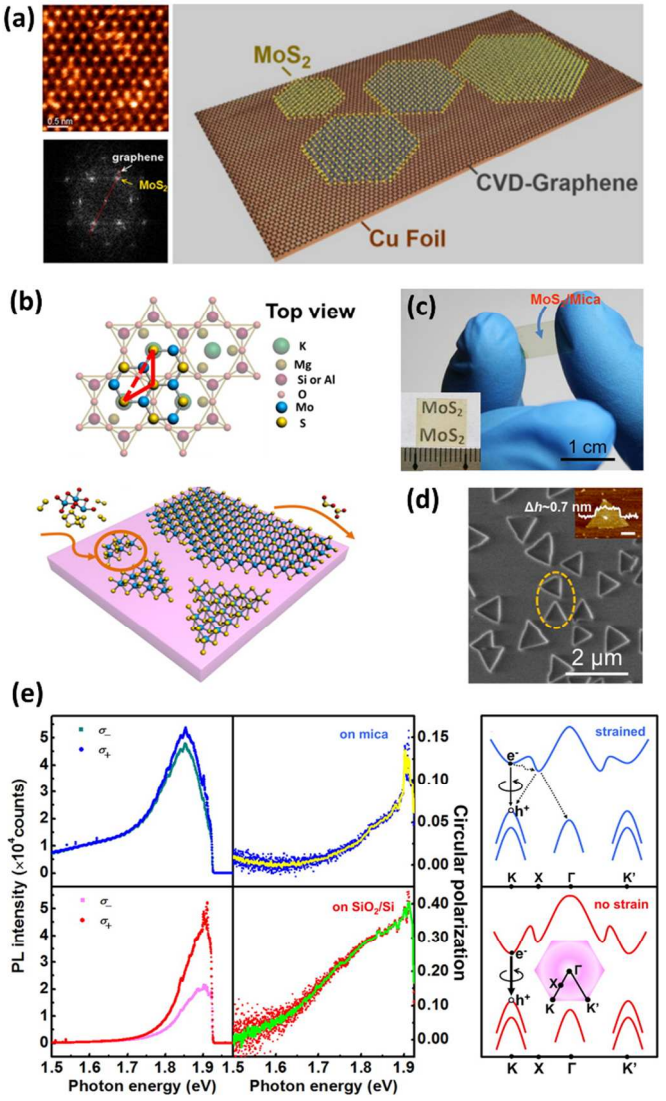

Fig. 9 (a) TEM analysis of monolayer MoS_2 grown on graphene. The electron diffraction pattern suggests the van der Waals epitaxy of MoS_2/graphene layers. [62] Reproduced with permission from ref. 62.Copyright 2012 American Chemical Society (b) A schematic view illustrating the surface reaction during epitaxial growth of MoS_2. [65] (c) Photograph of monolayer MoS_2 with a full coverage on mica. [65] (d) Magnified SEM image displaying the distribution of MoS_2 layers on mica. Inset shows the AFM image of the highlighted part in figure. [65] (e). Valley-polarized emission from as-grown monolayer MoS_2 on mica and after transfer to SiO_2/Si substrates. The complementary coloured curves are adjacent-point-averaged results of circular polarization. Figure on the right shows the schematic band structure along K-Γ-K′ direction for the compressively strained (top) and zero strained monolayer MoS_2 (bottom). Only the direct-gap emission at K valley (solid arrow) shows helicity and the indirect-gap transitions (marked with dashed arrows) give nonpolarized emissions. [65] Reproduced with permission from ref. 65. Copyright 2013 American Chemical Society

for the MoS_2/graphene van der Waals stacking layers, all the remaining strain is expected to get accommodated in the van der Waals (vdW) gap. Therefore, even though there is a large lattice mismatch between the MoS_2 and graphene structure, it was found that graphene can serve as an epitaxial substrate for MoS_2 (Fig. 9a). The heterostructures of graphene/MoS_2 hybrids show great potential in the hydrogen evolution reaction (HER).[63, 64]

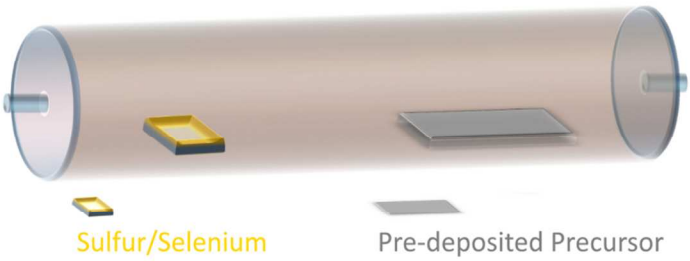

TMDs	Precursors	Growth condition	Morphology	Optical/ Electrical Properties	Remarks
Thermolysis of Pre-deposited Thiosalt					
MoS_2	$(NH_4)_2MoS_4$, Sulfur powder	1 to 500 Torr, 500-1000 °C	Bilayer and trilayer thin film	Bottom gate FET: On/Off ratio: 1.6×10^5 Mobility: 6 $cm^2V^{-1}s^{-1}$	Ref. 30
	$(NH_4)_2MoS_4$, Sulfur powder	1 to 500 Torr, 500-1000 °C	Bilayer and trilayer thin film	Electric double-layer FET: Low threshold voltage <1 V; High Mobility: 12.5 $cm^2V^{-1}s^{-1}$	Ref. 11, 31
MoS_2/Graphene	$(NH_4)_2MoS_4$	10 mTorr to Atmosphere, 400 °C	few layer TMDs on graphene		Ref. 62
Sulfurization/Selenization of Pre-deposited TMD layers					
$MoS_{2(1-x)}Se_{2x}$ ($0 \le x \le 0.40$)	MoS_2 layers (CVD synthesized), Selenium powder (heating at 270 °C)	Atmosphere, 600 to 900°C	$MoS_{2x}Se_{2(1-x)}$ monolayer alloys	Optical band gap tunable from 1.57 (790 nm) to 1.86 eV (667 nm)	Ref.55
$MoS_{2(1-x)}Se_{2x}$ ($0 \le x \le 0.40$)	CVD synthesized MoS_2 /$MoSe_2$ layers, Sulfur powder (heating at 160°C), Selenium powder(heating at 270°C)	Atmosphere, 600 to 900°C	$MoS_{2x}Se_{2(1-x)}$ monolayer alloys	Band gap photoluminescence is tunable from 1.57 eV (790 nm) to 2.0 eV (620 nm)	Ref. 56
Sulfurization/Selenization of Pre-deposited Metal thin film/Metal Oxide					
MoS_2	~1- 5 nm Mo film, Sulfur powder (heating at >113 °C)	Atmosphere at 500-750 °C	Continues thin film with monolayer and few layer TMDs coexist	Field-effect transistor (FET): Mobility: 0.004 to 0.04 $cm^2V^{-1}s^{-1}$ Resistivity: ~1.46×10^4 to 2.84×10^4 Ω/□	Ref. 24
	~0.8 to 3.6 nm MoO_3 thin layer, Sulfur powder (heating together with precursor at 1000 °C)	1 to 600 Torr, 500 to 1000 °C	2 to 3 layers isolated domains, 3 layers continuous film	FET: On/Off ratio: 10^5 Mobility: 0.8$cm^2V^{-1}s^{-1}$	Ref. 26 Capable for wafer scale synthesis of TMDs
	MoO_2 microcrystals (MoO_3 reduced by Sulfur at 650 to 850 °C), sulfur powder(heating at 145 °C)	Atmosphere, 850 to 950 °C	Rhomboidal shape TMD layers	FET: On/Off ratio: 10^4 to 10^6 Mobility: 0.1 to 0.7 $cm^2V^{-1}s^{-1}$	Ref. 29 Layer by layer sulfurization of Metal oxides
MoS_2, $MoSe_2$	5 nm Mo film, Sulfur powder (heating at 220 °C) Selenium powder (heating at 300 °C)	Low pressure, 550 °C	MoS_2 and $MoSe_2$ Films with Vertically Aligned Layers	Catalyst for hydrogen evolution reaction: Exchange current density (A/cm^2) MoS_2: 2.2×10^{-6} $MoSe_2$: 2.0×10^{-6}	Ref. 25 The edge-terminated films are metastable structures TMDs
WSe_2	5 nm WO_3, Selenium powder (heating at 500)	Atmosphere, 800 °C	WSe_2 Grown on Graphene/SiC		Ref. 60
WS_2	WO_3 thin by atomic layer deposition (ALD), H_2S gas	Atmosphere, 470 to 1000 °C	Mono-,bi-, and tetralayers, WS_2 nanotubes	FET: Using high-k dielectric as gate Insulator (50 nm HfO_2) Mobility:3.90 $cm^2V^{-1}s^{-1}$	Ref. 28
	~1 to 2.8 nm WO_X thin film, Sulfur powder (heating at 200°C)	450 mTorr, 750 to 900 °C; Atmosphere for few layer TMDs synthesis	Mono-,bi-, trilayer WS_2		Ref. 27 $W_xMo_yS_2$ can also be produced by MoO_x and Wo_x coated substrates

Table. 1 Summary of vapour phase sulfurization/ selenization method

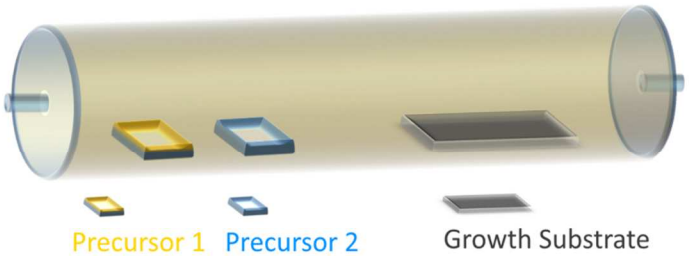

Vapor Phase Reaction					
TMDs	Precursors	Growth condition	Morphology	Optical/ Electrical Properties	Remarks
MoS_2	MoO_3 Sulfur Powder	Atmosphere, 650 °C	Monolayer	FET: On/Off ratio: ~10^4 Mobility: 0.02$cm^2V^{-1}s^{-1}$	Ref. 32 Graphene-like molecules were used for substrate treatment
	MoO_3, Sulfur Powder (heating at 180 °C)	Atmosphere, 650 °C	Monolayer		Ref.34 Various of aromatic molecules can be used as seeding promoters
	MoO_3 nanoribbons Sulfur Powder	Atmosphere, 850 °C	Monolayer	FET: On/Off ratio: ~6×10^6 Mobility: ~4.3 $cm^2V^{-1}s^{-1}$	Ref. 35 Patterned substrates were used to control the nucleation
	MoO_3 Sulfur Powder	Atmosphere, 700 °C	Monolayer	FET: On/Off ratio: ~1×10^5 to 1×10^7 Mobility: ~3 to 4 $cm^2V^{-1}s^{-1}$	Ref. 36 Large single domain (> 100 μm) can be synthesized by using ultraclean substrates
	$MoCl_3$, Sulfur Powder (heating at 300°C)	2 Torr, 850 °C	Monolayer and fewlayer	FET: Mobility: ~0.003 to 0.03 $cm^2V^{-1}s^{-1}$	Ref.37
	MoO3, Sulfur Powder (heating at ~100°C)	~225 mTorr, 530 °C	Monolayer on Mica	Perfect valley related optical properties	Ref. 65
	MoO_3, Sulfur Powder (heating at ~130°C)	5 Torr, 670 °C	Monolayer on Graphene/SiC	10^3 improvement in photoresponse compared to MoS_2 along	Ref. 60
WS_2	WO_3 Sulfur Powder	550 to 750 °C	Monolayer		Ref. 5
	WO_3 Sulfur Powder (heating at ~100°C)	~225 mTorr, 900 °C	Monolayer and fewlayer	FET: On/Off ratio: ~1×10^2 Mobility: ~0.46 and 0.28 $cm^2V^{-1}s^{-1}$ for electron and hole ,respectively	Ref. 39 Ionic liquid used as the gating dielectric H_2 can tailor the shape of monolayer WS_2
WS_2, MoS_2	MoO_3, WO_3 Sulfur Powder	Atmosphere, 650 °C	Monolayer	MoS_2 FET: On/Off ratio: >10^7 Mobility: 1.2$cm^2V^{-1}s^{-1}$ WS_2 FET: On/Off ratio: >10^5 Mobility: 0.01 $cm^2V^{-1}s^{-1}$	Ref. 33 Small molecules were used as seeding for growth Low mobility of WS_2 could be due to the non-optimised metal electrodes
$MoSe_2$	MoO_3 powder, Selenium powder (heating at~ 300°C)	Atmosphere, 750 °C	Monolayer and fewlayer		Ref. 41
WSe_2	WO_3 powder (heating at 925 °C), Selenium powder (heating at~ 270°C)	Atmosphere, 750 to 850 °C	Monolayer	Electric double-layer FET: p channel: On/Off ratio: ~10^5 Mobility: 90 $cm^2V^{-1}s^{-1}$ n channel: On/Off ratio: ~10^4 Mobility: 7 $cm^2V^{-1}s^{-1}$ WSe_2 based invert exhibits a high gain of ~13	Ref. 42
$MoS_{2(1-x)}Se_{2x}$	MoO_3 Sulfur and Selenium Powder	Atmosphere, ~800 °C	Monolayer	Optical band gap can be fine tuned between 1.85 and 1.60 eV	Ref. 53

Table. 2 Summary of vapor phase reaction method

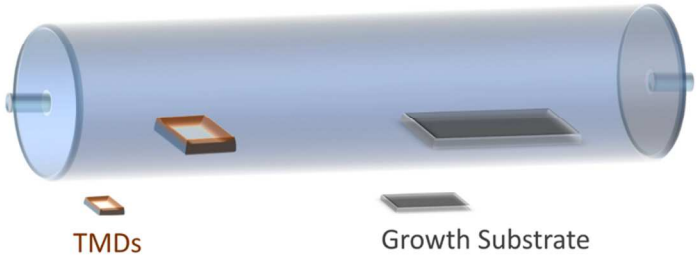

Vapor Phase Transport					
TMDs	Precursors	Growth condition	Morphology	Optical/ Electrical Properties	Remarks
MoS_2	MoS_2 powder	20 torr, 900 °C	Monolayer and few layer TMDs	The photoluminescence polarization is substantial with a maximum of 35% at ~1.92 eV, at room temperature	Ref. 44
$MoS_{2(1-x)}Se_{2x}$ ($0 \le x \le 0.40$)	MoS_2 and $MoSe_2$ powders (heating at 940-975 °C)	~60 mTorr, 600-700 °C	Monolayer	Band gap photoluminescence is tunable from 1.86 eV (i.e., 665 nm, reached with x = 0) to 1.73 eV (i.e., 716 nm, reached with x = 0.40). Average FET mobility: 0.1 to 0.4 $cm^2V^{-1}s^{-1}$	Ref. 54

Table. 3 Summary of vapour phase transport method

Besides graphene, fluorophlogopite mica ($KMg_3AlSi_3O_{10}F_2$) is also considered to be a good vdW expitaxy substrate for TMD growth due to their atomic flat and chemically inert surface with a hexagonally arranged in-plane lattice.[65] Ji *et al*. reported centimetre-scale uniform monolayer MoS_2 can be synthesized on mica through low-pressure CVD (LPCVD) process (Fig 9. b-e).[65] It was concluded that the MoS_2 growth on mica follows an analogous layer-plus-island (or Stranski-Krastanov) growth mode. The Stranski-Krastanov mode follows a two-step process: initially, monolayer MoS_2 domains gather and interconnect with each other till the full coverage of monolayer is nearly completed. Beyond the critical layer number (1 for MoS_2 on mica), the growth of MoS_2 continues through the nucleation and coalescence of MoS_2 nanoparticles or few layers islands. Meanwhile, the epitaxial monolayer MoS_2 grown on mica is intrinsically strained due to a small adlayer-substrate lattice mismatch.[65] Room-temperature PL helicity can also be observed when MoS_2 layers are transferred to SiO_2/Si substrate where the intrinsic strain gets released. The results are similar to the optical quality MoS_2 obtained by vapour-solid method,[44] suggesting the high crystal quality of the MoS_2 synthesized by combining vdW epitaxy with LPCVD.

Conclusions

This review provides a largely collection of literatures for the preparation of various TMD materials. Table 1, 2 and 3 list the common methods for TMDs synthesis. The reported synthesis conditions and the key properties, such as morphology, number of layers, mobilities, optical band gap have been sumarized. Typical experimental setup has also been schematically illustrated. The semiconducting TMD materials with a tuneable doping level make them complementary to graphene. Vapour deposition methods have been developed for the synthesis of monolayer and few-layer TMD nanosheets such as MoS_2, WS_2, WSe_2 and $MoSe_2$. The CVD approaches, suitable for wafer scale fabrication, provide high-quality TMD films useful for electronic and optoelectronic devices. In addition, the electro dispersive property and the semiconducting nature of 2D TMDs can be tailored by bandgap engineering. The stacking of different types of 2D nanomateirals also attracts attention for integrated circuits. Novel properties and new phenomena could arise from the 2D heterostructural stacking or alloys. To realize the practical applications, more efforts are needed to attack many issues related to the growth, including layer number control, size control, area selective growth and the direct growth of heterostructures.

Acknowledgements

YS and LJL thank the support from King Abdullah University of Science and Technology.

Notes and references

a Physical Sciences and Engineering, King Abdullah University of Science and Technology, Thuwal, 23955-6900, Kingdom of Saudi Arabia.
b School of Materials Science and Engineering, Nanyang Technological University, Block N4.1, Nanyang Avenue, Singapore 639798

1. RadisavljevicB, RadenovicA, BrivioJ, GiacomettiV and KisA, *Nat Nano*, 2011, **6**, 147-150.
2. O. Lopez-Sanchez, D. Lembke, M. Kayci, A. Radenovic and A. Kis, *Nat Nano*, 2013, **8**, 497-501.
3. H. Zeng, J. Dai, W. Yao, D. Xiao and X. Cui, *Nat Nano*, 2012, **7**, 490-493.
4. W. Zhang, C.-P. Chuu, J.-K. Huang, C.-H. Chen, M.-L. Tsai, Y.-H. Chang, C.-T. Liang, Y.-Z. Chen, Y.-L. Chueh, J.-H. He, M.-Y. Chou and L.-J. Li, *Sci. Rep.*, 2014, **4**, 3826.
5. C. Cong, J. Shang, X. Wu, B. Cao, N. Peimyoo, C. Qiu, L. Sun and T. Yu, *Advanced Optical Materials*, 2014, **2**, 131-136.
6. Y. Cai, J. Lan, G. Zhang and Y.-W. Zhang, *Physical Review B*, 2014, **89**, 035438.
7. S. Bertolazzi, J. Brivio and A. Kis, *ACS Nano*, 2011, **5**, 9703-9709.

8. M. Chhowalla, H. S. Shin, G. Eda, L.-J. Li, K. P. Loh and H. Zhang, *Nat Chem*, 2013, **5**, 263-275.
9. X. Huang, Z. Zeng and H. Zhang, *Chemical Society Reviews*, 2013, **42**, 1934-1946.
10. H. Wang, L. Yu, Y.-H. Lee, Y. Shi, A. Hsu, M. L. Chin, L.-J. Li, M. Dubey, J. Kong and T. Palacios, *Nano Letters*, 2012, **12**, 4674-4680.
11. J. Pu, Y. Yomogida, K.-K. Liu, L.-J. Li, Y. Iwasa and T. Takenobu, *Nano Letters*, 2012, **12**, 4013-4017.
12. F. K. Perkins, A. L. Friedman, E. Cobas, P. M. Campbell, G. G. Jernigan and B. T. Jonker, *Nano Letters*, 2013, **13**, 668-673.
13. H. Li, Z. Yin, Q. He, H. Li, X. Huang, G. Lu, D. W. H. Fam, A. I. Y. Tok, Q. Zhang and H. Zhang, *Small*, 2012, **8**, 63-67.
14. Z. Yin, H. Li, H. Li, L. Jiang, Y. Shi, Y. Sun, G. Lu, Q. Zhang, X. Chen and H. Zhang, *ACS Nano*, 2011, **6**, 74-80.
15. W. Zhang, J.-K. Huang, C.-H. Chen, Y.-H. Chang, Y.-J. Cheng and L.-J. Li, *Advanced Materials*, 2013, **25**, 3456-3461.
16. K. Roy, M. Padmanabhan, S. Goswami, T. P. Sai, G. Ramalingam, S. Raghavan and A. Ghosh, *Nat Nano*, 2013, **8**, 826-830.
17. L. Yu, Y.-H. Lee, X. Ling, E. J. G. Santos, Y. C. Shin, Y. Lin, M. Dubey, E. Kaxiras, J. Kong, H. Wang and T. Palacios, *Nano Letters*, 2014, **14**, 3055-3063.
18. H. Schmidt, S. Wang, L. Chu, M. Toh, R. Kumar, W. Zhao, A. H. Castro Neto, J. Martin, S. Adam, B. Özyilmaz and G. Eda, *Nano Letters*, 2014, **14**, 1909-1913.
19. G.-H. Lee, Y.-J. Yu, X. Cui, N. Petrone, C.-H. Lee, M. S. Choi, D.-Y. Lee, C. Lee, W. J. Yoo, K. Watanabe, T. Taniguchi, C. Nuckolls, P. Kim and J. Hone, *ACS Nano*, 2013, **7**, 7931-7936.
20. G. Eda, H. Yamaguchi, D. Voiry, T. Fujita, M. Chen and M. Chhowalla, *Nano Letters*, 2011, **11**, 5111-5116.
21. A. O'Neill, U. Khan and J. N. Coleman, *Chemistry of Materials*, 2012, **24**, 2414-2421.
22. Z. Zeng, T. Sun, J. Zhu, X. Huang, Z. Yin, G. Lu, Z. Fan, Q. Yan, H. H. Hng and H. Zhang, *Angewandte Chemie International Edition*, 2012, **51**, 9052-9056.
23. H. Li, J. Wu, Z. Yin and H. Zhang, *Accounts of Chemical Research*, 2014, **47**, 1067-1075.
24. Y. Zhan, Z. Liu, S. Najmaei, P. M. Ajayan and J. Lou, *Small*, 2012, **8**, 966-971.
25. D. Kong, H. Wang, J. J. Cha, M. Pasta, K. J. Koski, J. Yao and Y. Cui, *Nano Letters*, 2013, **13**, 1341-1347.
26. Y.-C. Lin, W. Zhang, J.-K. Huang, K.-K. Liu, Y.-H. Lee, C.-T. Liang, C.-W. Chu and L.-J. Li, *Nanoscale*, 2012, **4**, 6637-6641.
27. A. L. Elías, N. Perea-López, A. Castro-Beltrán, A. Berkdemir, R. Lv, S. Feng, A. D. Long, T. Hayashi, Y. A. Kim, M. Endo, H. R. Gutiérrez, N. R. Pradhan, L. Balicas, T. E. Mallouk, F. López-Urías, H. Terrones and M. Terrones, *ACS Nano*, 2013, **7**, 5235-5242.
28. J.-G. Song, J. Park, W. Lee, T. Choi, H. Jung, C. W. Lee, S.-H. Hwang, J. M. Myoung, J.-H. Jung, S.-H. Kim, C. Lansalot-Matras and H. Kim, *ACS Nano*, 2013, **7**, 11333-11340.
29. X. Wang, H. Feng, Y. Wu and L. Jiao, *Journal of the American Chemical Society*, 2013, **135**, 5304-5307.
30. K.-K. Liu, W. Zhang, Y.-H. Lee, Y.-C. Lin, M.-T. Chang, C.-Y. Su, C.-S. Chang, H. Li, Y. Shi, H. Zhang, C.-S. Lai and L.-J. Li, *Nano Letters*, 2012, **12**, 1538-1544.
31. J. Pu, Y. Zhang, Y. Wada, J. Tse-Wei Wang, L.-J. Li, Y. Iwasa and T. Takenobu, *Applied Physics Letters*, 2013, **103**, 023505.
32. Y.-H. Lee, X.-Q. Zhang, W. Zhang, M.-T. Chang, C.-T. Lin, K.-D. Chang, Y.-C. Yu, J. T.-W. Wang, C.-S. Chang, L.-J. Li and T.-W. Lin, *Advanced Materials*, 2012, **24**, 2320-2325.
33. Y.-H. Lee, L. Yu, H. Wang, W. Fang, X. Ling, Y. Shi, C.-T. Lin, J.-K. Huang, M.-T. Chang, C.-S. Chang, M. Dresselhaus, T. Palacios, L.-J. Li and J. Kong, *Nano Letters*, 2013, **13**, 1852-1857.
34. X. Ling, Y.-H. Lee, Y. Lin, W. Fang, L. Yu, M. S. Dresselhaus and J. Kong, *Nano Letters*, 2014, **14**, 464-472.
35. S. Najmaei, Z. Liu, W. Zhou, X. Zou, G. Shi, S. Lei, B. I. Yakobson, J.-C. Idrobo, P. M. Ajayan and J. Lou, *Nat Mater*, 2013, **12**, 754-759.
36. A. M. van der Zande, P. Y. Huang, D. A. Chenet, T. C. Berkelbach, Y. You, G.-H. Lee, T. F. Heinz, D. R. Reichman, D. A. Muller and J. C. Hone, *Nat Mater*, 2013, **12**, 554-561.
37. Y. Yu, C. Li, Y. Liu, L. Su, Y. Zhang and L. Cao, *Sci. Rep.*, 2013, **3**, 1866.
38. H. R. Gutiérrez, N. Perea-López, A. L. Elías, A. Berkdemir, B. Wang, R. Lv, F. López-Urías, V. H. Crespi, H. Terrones and M. Terrones, *Nano Letters*, 2012, **13**, 3447-3454.
39. Y. Zhang, Y. Zhang, Q. Ji, J. Ju, H. Yuan, J. Shi, T. Gao, D. Ma, M. Liu, Y. Chen, X. Song, H. Y. Hwang, Y. Cui and Z. Liu, *ACS Nano*, 2013, **7**, 8963-8971.
40. X. Wang, Y. Gong, G. Shi, W. L. Chow, K. Keyshar, G. Ye, R. Vajtai, J. Lou, Z. Liu, E. Ringe, B. K. Tay and P. M. Ajayan, *ACS Nano*, 2014, **8**, 5125-5131.
41. J. Shaw, H. Zhou, Y. Chen, N. Weiss, Y. Liu, Y. Huang and X. Duan, *Nano Res.*, 2014, **7**, 1-7.
42. J.-K. Huang, J. Pu, C.-L. Hsu, M.-H. Chiu, Z.-Y. Juang, Y.-H. Chang, W.-H. Chang, Y. Iwasa, T. Takenobu and L.-J. Li, *ACS Nano*, 2013, **8**, 923-930.
43. C. Mai, A. Barrette, Y. Yu, Y. G. Semenov, K. W. Kim, L. Cao and K. Gundogdu, *Nano Letters*, 2013, **14**, 202-206.
44. S. Wu, C. Huang, G. Aivazian, J. S. Ross, D. H. Cobden and X. Xu, *ACS Nano*, 2013, **7**, 2768-2772.
45. A. Castellanos-Gomez, R. Roldán, E. Cappelluti, M. Buscema, F. Guinea, H. S. J. van der Zant and G. A. Steele, *Nano Letters*, 2013, **13**, 5361-5366.
46. H. J. Conley, B. Wang, J. I. Ziegler, R. F. Haglund, S. T. Pantelides and K. I. Bolotin, *Nano Letters*, 2013, **13**, 3626-3630.
47. Y. Y. Hui, X. Liu, W. Jie, N. Y. Chan, J. Hao, Y.-T. Hsu, L.-J. Li, W. Guo and S. P. Lau, *ACS Nano*, 2013, **7**, 7126-7131.
48. J. Mann, Q. Ma, P. M. Odenthal, M. Isarraraz, D. Le, E. Preciado, D. Barroso, K. Yamaguchi, G. von Son Palacio, A. Nguyen, T. Tran, M. Wurch, A. Nguyen, V. Klee, S. Bobek, D. Sun, T. F. Heinz, T. S. Rahman, R. Kawakami and L. Bartels, *Advanced Materials*, 2014, **26**, 1399-1404.
49. G. H. Yousefi and M. K. Agarwal, *J Mater Sci Lett*, 1993, **12**, 1731-1732.

50. M. Zhang, J. Wu, Y. Zhu, D. O. Dumcenco, J. Hong, N. Mao, S. Deng, Y. Chen, Y. Yang, C. Jin, S. H. Chaki, Y.-S. Huang, J. Zhang and L. Xie, *ACS Nano*, 2014, **8**, 7130-7137.
51. Y. Chen, J. Xi, D. O. Dumcenco, Z. Liu, K. Suenaga, D. Wang, Z. Shuai, Y.-S. Huang and L. Xie, *ACS Nano*, 2013, **7**, 4610-4616.
52. D. O. Dumcenco, K. Y. Chen, Y. P. Wang, Y. S. Huang and K. K. Tiong, *Journal of Alloys and Compounds*, 2010, **506**, 940-943.
53. Y. Gong, Z. Liu, A. R. Lupini, G. Shi, J. Lin, S. Najmaei, Z. Lin, A. L. Elías, A. Berkdemir, G. You, H. Terrones, M. Terrones, R. Vajtai, S. T. Pantelides, S. J. Pennycook, J. Lou, W. Zhou and P. M. Ajayan, *Nano Letters*, 2013, **14**, 442-449.
54. Q. Feng, Y. Zhu, J. Hong, M. Zhang, W. Duan, N. Mao, J. Wu, H. Xu, F. Dong, F. Lin, C. Jin, C. Wang, J. Zhang and L. Xie, *Advanced Materials*, 2014, **26**, 2648-2653.
55. S.-H. Su, Y.-T. Hsu, Y.-H. Chang, M.-H. Chiu, C.-L. Hsu, W.-T. Hsu, W.-H. Chang, J.-H. He and L.-J. Li, *Small*, 2014, **10**, 2589-2594.
56. H. W. Su S, Hsu C, Chen C, Chiu M, Lin Y, Chang W, Suenaga K, He J and Li L *Front. Energy Res.*, 2014, **2**, 27.
57. S. Tongay, W. Fan, J. Kang, J. Park, U. Koldemir, J. Suh, D. S. Narang, K. Liu, J. Ji, J. Li, R. Sinclair and J. Wu, *Nano Letters*, 2014, **14**, 3185-3190.
58. S. Bertolazzi, D. Krasnozhon and A. Kis, *ACS Nano*, 2013, **7**, 3246-3252.
59. M. Sup Choi, G.-H. Lee, Y.-J. Yu, D.-Y. Lee, S. Hwan Lee, P. Kim, J. Hone and W. Jong Yoo, *Nat Commun*, 2013, **4**, 1624.
60. Y.-C. Lin, N. Lu, N. Perea-Lopez, J. Li, Z. Lin, X. Peng, C. H. Lee, C. Sun, L. Calderin, P. N. Browning, M. S. Bresnehan, M. J. Kim, T. S. Mayer, M. Terrones and J. A. Robinson, *ACS Nano*, 2014, **8**, 3715-3723.
61. P. T. K. Loan, W. Zhang, C.-T. Lin, K.-H. Wei, L.-J. Li and C.-H. Chen, *Advanced Materials*, 2014, **26**, 4838-4844.
62. Y. Shi, W. Zhou, A.-Y. Lu, W. Fang, Y.-H. Lee, A. L. Hsu, S. M. Kim, K. K. Kim, H. Y. Yang, L.-J. Li, J.-C. Idrobo and J. Kong, *Nano Letters*, 2012, **12**, 2784-2791.
63. D. Voiry, M. Salehi, R. Silva, T. Fujita, M. Chen, T. Asefa, V. B. Shenoy, G. Eda and M. Chhowalla, *Nano Letters*, 2013, **13**, 6222-6227.
64. Y.-H. Chang, C.-T. Lin, T.-Y. Chen, C.-L. Hsu, Y.-H. Lee, W. Zhang, K.-H. Wei and L.-J. Li, *Advanced Materials*, 2013, **25**, 756-760.
65. Q. Ji, Y. Zhang, T. Gao, Y. Zhang, D. Ma, M. Liu, Y. Chen, X. Qiao, P.-H. Tan, M. Kan, J. Feng, Q. Sun and Z. Liu, *Nano Letters*, 2013, **13**, 3870-3877.

